

Multifractality in the interacting disordered Tavis-Cummings model

F. Mattiotti,¹ J. Dubail,^{1,2} D. Hagenmüller,¹ J. Schachenmayer,¹ J.-P. Brantut,^{3,4} and G. Pupillo^{1,5}

¹*University of Strasbourg and CNRS, CESQ and ISIS (UMR 7006), aQCeSS, 67000 Strasbourg, France*

²*Université de Lorraine and CNRS, LPCT (UMR 7019), 54000 Nancy, France*

³*Ecole Polytechnique Fédérale de Lausanne, Institute of Physics, CH-1015 Lausanne, Switzerland*

⁴*Center for Quantum Science and Engineering, Ecole Polytechnique Fédérale de Lausanne, CH-1015 Lausanne, Switzerland*

⁵*Institut Universitaire de France (IUF), 75000 Paris, France*

We analyze the spectral and transport properties of the interacting disordered Tavis-Cummings model at half excitation filling. We demonstrate that a poissonian level statistics coexists with eigenfunctions that are multifractal (extended, but non-ergodic) in the Hilbert space, for all strengths of light-matter interactions. This is associated with a lack of thermalization for a local perturbation, which remains partially localized in the infinite-time limit. We argue that these effects are due to the combination of finite interactions and integrability of the model. When a small integrability-breaking perturbation (nearest-neighbour hopping) is introduced, typical eigenfunctions become ergodic, seemingly turning the system into a near-perfect conductor, contrary to the single-excitation non-interacting case. We propose a realization of this model with cold atoms.

Introduction. Multifractality is a generalization of the concept of a fractal object – usually characterized by a single fractal dimension – to scale-invariant probability distributions characterized by a continuous spectrum of fractal dimensions [1]. Multifractality plays an important role in a wide variety of situations including earth topography [2], turbulent flows [3], heartbeat dynamics [4], and financial markets [5]. Another example is the case of Anderson metal-insulator transitions in disordered quantum systems [6], where multifractality is known to be a meaningful feature of the critical wavefunctions connected to a characteristic (semi-Poissonian) distribution of consecutive energy levels and a multifractal spectrum that identifies the universality class of the transition [7–10]. In these systems, multifractality reflects the extended, yet non-ergodic, nature of the eigenstates, which is usually associated with finite, however limited conductivity. This is in contrast to good conductors and insulating phases where eigenstates are fully ergodic and fully non-ergodic, respectively, and energy levels are distributed according to different characteristic (Wigner-Dyson, Poissonian) distributions [7]. Beyond single-particle wavefunctions, multifractal behavior has been recently reported in strongly interacting disordered quantum systems in connection with many-body localization (MBL) [11–15], and in certain random matrix models [16–19] that serve as toy models for quantum chaos [10]. The precise connection between interactions, multifractality, level statistics and transport properties as well as experimental realizations of multifractal behavior in any interacting quantum many-body systems have so-far remained largely elusive.

In this work we demonstrate that multifractal eigenstates are found in interacting disordered quantum many-body spin systems coupled to a delocalized bosonic mode. We consider the Tavis-Cummings (TC) model of cavity quantum electrodynamics [20], that describes N two-level quantum emitters – or (pseudo) spins – coupled to a sin-

gle cavity mode (Fig. 1a). We consider that model in the presence of disorder in the local Zeeman energies of the spins, a form of diagonal disorder that is common when the transition frequencies of the two-level systems are inhomogeneously broadened [21–24]. The total number of excitations M (number of excitons+photons) is conserved in the TC model; here we focus on half-filling ($M = N/2$) as a prototypical example of a finite density of excitations in the thermodynamic limit ($N \rightarrow \infty$). We numerically demonstrate that, for all strengths of the light-matter interaction, the eigenstates of the TC Hamiltonian are multifractal in the computational basis. In contrast to the single-excitation case [8, 25], multifractality in the many-body Hilbert space is associated to a qualitatively different energy level statistics: while Poisson level statistics is usually associated to fully localized eigenstates, here we simultaneously observe Poisson statistics and multifractal – extended – eigenstates [a similar phenomenon has been pointed out recently in certain power-law banded random matrix models [26]]. We numerically demonstrate that interactions qualitatively change the nature of the eigenstates with respect to the single-particle case, favoring delocalization in the Hilbert space. We also analyze the microcanonical Edwards-Anderson (EA) order parameter introduced in Ref. [27] which probes thermalization of single-spin excitations in the infinite-time limit. We find a non-vanishing EA parameter, signaling the absence of such thermalization, for all light-matter interaction strengths. Interestingly, our findings show that the disordered TC model possesses various known features of MBL phases, including Poisson statistics [28, 29], lack of thermalization [30, 31], and multifractality of the eigenstates [12, 14, 32]. However, unlike MBL, these features are found to be unstable towards a small breaking of integrability. We show this by adding a weak nearest-neighbor Hamiltonian hopping term between excitons, which turns the interacting multifractal phase into a perfect conductor for typical energies

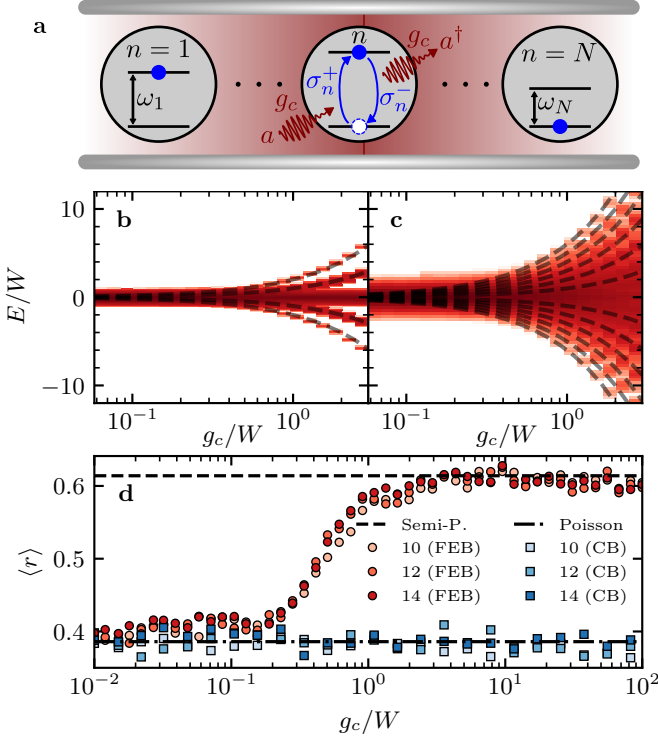


FIG. 1. **a** The Tavis-Cummings (TC) model [Eq. (1)]: N two-level system (or pseudo-spins), with disorder in their transition energies ω_n , are coupled to the same mode of an optical cavity, with collective coupling strength g_c . Multiple excitations can be present, either in the two-level systems (blue circles) or as photons in the cavity. **b,c** Density of states of the TC model (1) for $N = 12$ as a function of the energy E and of the coupling g_c , in units of the disorder strength W . Each panel represents different numbers of excitations: $M = 2$ (**b**) and $M = 6$ (**c**). The dashed lines represent the low-excitation-density approximation ($M \ll N$): jg_c , with $j = -M, \dots, M$. **d** Mean level spacing ratio [Eq. (4)] for the first-excited energy band (FEB) and for the central energy band (CB) for $N/2$ excitations in N sites (N indicated in the legend). The semi-Poisson value (dashed line) has been computed numerically [33], while the Poisson value ($2 \ln 2 - 1$, dash-dotted line) is known [34–36].

in the middle of the spectrum, while the low-energy states remain multifractal. This is in contrast to the single particle case, which is robust with respect to this perturbation [25]. We propose below a protocol to experimentally analyze this physics with ultra-cold atoms.

Model. The TC Hamiltonian for N quantum emitters coupled to a single bosonic mode in the rotating wave approximation reads ($\hbar = 1$)

$$H_{\text{TC}} = \sum_{n=1}^N \omega_n \sigma_n^+ \sigma_n^- + \frac{g_c}{\sqrt{N}} \sum_{n=1}^N (a^\dagger \sigma_n^- + \sigma_n^+ a) , \quad (1)$$

where $\omega_n \in [-W/2, W/2]$ are random, uniformly distributed energies (shifted by the cavity frequency), g_c is the collective coupling strength of the emitters to the cavity mode, σ_n^\pm are Pauli operators such that $[\sigma_n^-, \sigma_m^-] =$

$[\sigma_n^+, \sigma_m^+] = 0$, $[\sigma_n^+, \sigma_m^-] = \delta_{nm} \sigma_n^z$, and a^\dagger/a is the boson creation/annihilation operator with $[a, a^\dagger] = 1$. The number of excitations $M = \sum_{n=1}^N \sigma_n^+ \sigma_n^- + a^\dagger a$ is conserved. The (non-normalized) eigenstates of H are of the form [37–42]

$$|\lambda_1, \dots, \lambda_M\rangle = \Sigma^\dagger(\lambda_1) \cdots \Sigma^\dagger(\lambda_M) |0\rangle \quad (2)$$

where the raising operators $\Sigma^\dagger(\lambda) = a^\dagger + \frac{1}{\sqrt{N}} \sum_{n=1}^N g_c(\lambda - \omega_n)^{-1} \sigma_n^+$ act on the vacuum $|0\rangle$ (the state with no exciton and no photon), and where the coefficients $\lambda_1, \dots, \lambda_M$ satisfy a system of M coupled non-linear equations,

$$- \frac{N \lambda_i}{2g_c^2} + \frac{1}{2} \sum_{n=1}^N \frac{1}{\lambda_i - \omega_n} = \sum_{\substack{j=1 \\ j \neq i}}^M \frac{1}{\lambda_i - \lambda_j} . \quad (3)$$

[For $M = 1$, there is a single equation, equivalent to the secular equation of an arrowhead matrix, see Ref. [8].] Equations. (3) are called the ‘Bethe equations’, and they are a consequence of the underlying integrability of the model, see e.g. Refs. [37–42].

Energy bands. For low excitation density ($M \ll N$), the r.h.s. in Eq. (3) is negligible, and the coefficients λ_i approximately coincide with the eigenvalues of the $M = 1$ case [8]. For large coupling ($g_c \gg W$), these correspond to the two polaritons $\lambda_i \simeq \pm g_c$, or to one of the $N - 1$ dark states $\lambda_i \simeq \Omega_n := (\omega_{n+1} + \omega_n)/2$, where we assume w.l.o.g. that $\omega_1 < \omega_2 < \dots < \omega_N$. The corresponding operators are the polariton creation operators $\Sigma^\dagger(\pm g_c) \approx a^\dagger \pm \sum_{n=1}^N \sigma_n^+ / \sqrt{N}$ and the dark state creation operators $\Sigma^\dagger(\Omega_n) \approx (g_c / \sqrt{N}) \sum_{m=1}^N \sigma_m^+ / (\Omega_n - \omega_m)$, with $n = 1, \dots, N - 1$. For instance, for $M = 2$ excitations the approximate basis is formed by: (a) combinations of two polaritons, $[\Sigma^\dagger(\pm g_c)]^2 |0\rangle$ and $\Sigma^\dagger(g_c) \Sigma^\dagger(-g_c) |0\rangle$; (b) combinations of a polariton and a dark state, $\Sigma^\dagger(\pm g_c) \Sigma^\dagger(\Omega_n) |0\rangle$; (c) combinations of two different dark states, $\Sigma^\dagger(\Omega_n) \Sigma^\dagger(\Omega_{n'}) |0\rangle$. More generally, with M excitations at strong coupling, there are $2M + 1$ energy bands centered at jg_c , with $j = -M, \dots, M$. This prediction is compared to the numerical density of states in Fig. 1b,c for $N = 12$ (the dashed lines are for jg_c). Here, a low-density approximation works well for $M = 2$ (**b**), but fails for $M = 6$ at half filling (**c**). This discrepancy is expected, since the interaction effects are non-negligible at half filling. Nevertheless, the low-density description provides a general intuitive characterization of the many-body eigenstates for strong coupling. In particular, we focus our analysis on three sets of states that are good representatives of all the many-body states: the ground state (GS: $[\Sigma^\dagger(-g_c)]^M |0\rangle$), the first excited band (FEB, made of the 2nd-to- N^{th} excited states: $[\Sigma^\dagger(-g_c)]^{(M-1)} \Sigma^\dagger(\Omega_n) |0\rangle$), and the central band (CB: $\prod_{j=1}^M [\Sigma^\dagger(\Omega_j)] |0\rangle$). For the CB we select a small energy window made of the N states in the middle of the spectrum. The results presented below depend on the

energy band as long as they are well separated. At small coupling ($g_c \ll W$) the energy bands are merged into one single larger band (Fig. 1b,c).

Level statistics. In order to study the transport properties of the TC model, as a first step we analyze the statistics of the energy levels, since it is usually related to localization in many-body interacting systems [35, 36]. In order to analyze how the level statistics depends on the coupling strength, we compute the mean level spacing ratio [34–36]

$$\langle r \rangle = \left\langle \frac{\min(E_{n+1} - E_n, E_n - E_{n-1})}{\max(E_{n+1} - E_n, E_n - E_{n-1})} \right\rangle, \quad (4)$$

where E_n are the sorted eigenenergies. In Fig. 1d the mean level spacing ratio is plotted against the coupling to the cavity (FEB: circles, CB: squares) for half filling ($M = N/2$). As we discuss below, the CB is representative of many other energy bands, while the FEB has peculiar features. As one can see, the level statistics is Poissonian for small coupling for both bands, while for large coupling ($g_c \gg W$) the FEB reaches semi-Poissonian statistics and the CB remains Poissonian.

The different level statistics can be understood in terms of the previously introduced approximate characterization of the many-excitation eigenstates: indeed, the FEB energies are approximated as $-(M-1)g_c + \Omega_n$ and, therefore, keep the semi-Poisson statistics of the single-excitation energies Ω_n [8, 25]. On the other hand, the energies in the CB are $\approx \Omega_1 + \Omega_2 + \dots + \Omega_M$: since they result from the sum of random single-particle energies, they are independent random numbers, and thus show Poisson level statistics without level repulsion. Indeed, we have checked that also the other energy bands formed by more than one dark state show Poisson statistics.

Multifractality. We now proceed to analyze the delocalization of the many-body eigenfunctions in the Hilbert space by studying their multifractality. We define the generalized inverse participation ratio (IPR) in the many-body case (averaged in an energy window) as

$$\langle I_q \rangle = \left\langle \sum_{p=1}^{\mathcal{N}_M} |\langle p | E_\alpha \rangle|^{2q} \right\rangle \quad (5)$$

where $|p\rangle = (a^\dagger)^{n_p} \prod_{j=1}^{n_s} \sigma_j^+ |0\rangle$ are the many-excitation product states (eigenbasis for $g_c = 0$, with n_p photons and n_s spins, $n_s + n_p = M$) and $\mathcal{N}_M = \sum_{i=0}^M \binom{N}{i}$ is the size of the Hilbert space subset with M excitations. The average I_q is usually a power-law function of the Hilbert space size [7, 8, 12, 15]

$$\langle I_q \rangle \propto \mathcal{N}_M^{-\tau_q}, \quad (6)$$

where the exponent τ_q characterizes the delocalization. For instance, for fully extended (ergodic) eigenfunctions, one has $|\langle p | E_\alpha \rangle|^2 \sim O(\mathcal{N}_M^{-1})$ and therefore $\tau_q = q-1$. On

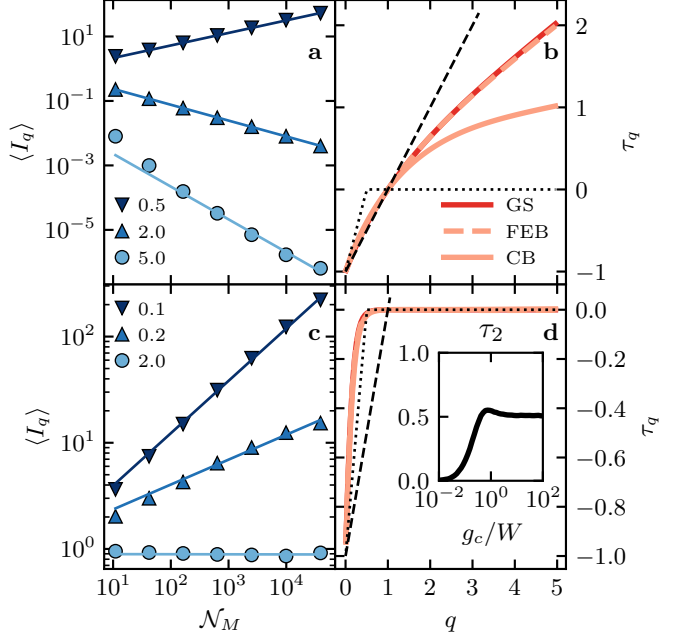


FIG. 2. **a,c** Average generalized IPR $\langle I_q \rangle$ [Eq. (5)] within the CB for different q values (see legends) as a function of the M -excitation Hilbert subspace size \mathcal{N}_M (corresponding to $N = 4, 6, 8, 10, 12, 14, 16$ respectively, with $M = N/2$), for $g_c/W = 10$ (**a**) and $g_c = 0.01$ (**c**). Lines: power-law fits $\propto \mathcal{N}_M^{-\tau_q}$. **b,d** Fitted exponent τ_q as a function of q for the ground state (GS), FEB and CB, for $g_c/W = 10$ (**b**) and $g_c = 0.01$ (**d**). GS' and FEB's data are overlapping in **b**, and all curves overlap in **d**. Black dashed line: fully extended case ($\tau_q = q-1$), dotted line: single-excitation case ($\tau_q = \min(2q-1, 0)$) [8]. Inset in (**d**): τ_2 , averaged over the full spectrum, as a function of the coupling strength.

the other hand, localized states feature one or few components $|\langle p | E_\alpha \rangle|^2 \sim O(1)$, implying $\tau_q = 0$. Any non-linear dependence on q identifies the system as multifractal [7].

In Fig. 2, τ_q is computed for strong ($g_c/W = 10$, see **a,b**) and weak coupling ($g_c/W = 0.01$, see **c,d**) by fitting $\langle I_q \rangle$ against \mathcal{N}_M at half filling, for different energy bands. The CB is shown in **a,c**, as an example, showing power-law relations between $\langle I_q \rangle$ and \mathcal{N}_M for any q . Similar power-law trends are observed also for the other energy bands, so that we determine τ_q by numerical fitting. The computed τ_q vs. q is shown in panel **b,d** for the GS, the FEB (whose results coincide with the GS) and the CB. Strong deviations from the ergodic case (dashed line) appear in all cases, indicating a clear multifractal behaviour both for strong (**b**) and weak (**d**) coupling, and for all the energy bands. For strong coupling, τ_q grows monotonically with q , similarly to what is observed in power-law banded random matrix models [7]. As the coupling decreases, τ_q approaches the single-excitation (non-interacting) case [8] (dotted line) for all the energy bands, with $\tau_q \approx 0$ for $q > 1/2$: such behaviour usually characterizes a transition to a ‘frozen

phase', that combines properties of localized and critical states [7]. However, here the multifractal character varies smoothly as a function of the coupling strength, with no clear sign of a phase transition. This is shown in the inset of Fig. 2d, where τ_2 (related to the standard IPR, I_2) averaged over the full spectrum is shown as a function of g_c/W . As the coupling increases, τ_2 grows and saturates to a finite value $\tau_2 \approx 0.5$, indicating that the eigenstates are multifractal for any coupling strength. This is in contrast to models showing many-body localization, where τ_2 is finite and non-unity only for strong disorder [12]. Interestingly, here the eigenfunctions are more delocalized than the corresponding non-interacting case [8].

Transport. So far our analysis has revealed that the TC model has Poisson level statistics, yet its eigenstates are not localized in the Hilbert space (see Ref. [26] for similar findings in a matrix model). To further characterize the transport properties of the model, we analyze the long-time survival probability, or microcanonical EA parameter, introduced in Ref. [27],

$$S = \frac{1}{\mathcal{N}_M} \sum_E \frac{1}{N} \sum_{n=1}^N |\langle E | \sigma_n^z | E \rangle|^2. \quad (7)$$

This parameter has a simple physical interpretation [27]. The system is initialized in an infinite temperature state with a small magnetization of spin n , $\langle \sigma_n^z \rangle_0 = \text{Tr}(\rho_0 \sigma_n^z) = \epsilon$, where the density matrix is $\rho_0 = (\mathbb{I} + \epsilon \sigma_n^z)/\mathcal{N}_M$. Then, the long-time local magnetization is $\langle \sigma_n^z \rangle_\infty = \lim_{t \rightarrow \infty} \text{Tr}(e^{-i\hat{H}t} \rho_0 e^{i\hat{H}t} \sigma_n^z) = \epsilon \sum_E |\langle E | \sigma_n^z | E \rangle|^2 / \mathcal{N}_M$. Therefore, Eq. (7) represents the ratio of the long-time local magnetization over the initial one, $\langle \sigma_n^z \rangle_\infty / \langle \sigma_n^z \rangle_0$, averaged over all the spins. Interestingly, in Ref. [27] it has been found that in the Richardson model – a related many-body spin model without a cavity mode and with all-to-all spin couplings – for any coupling strength, S remains finite in the thermodynamic limit. Such absence of thermalization has been related to the non-ergodicity of the many-body eigenfunctions. We perform the same analysis in the TC model, see Fig. 3a and observe that S saturates to a finite value when increasing N , for any finite coupling strength. Such value is close to unity for small coupling, indicating a nearly perfect insulator, and it decreases with g_c . However, in contrast to the Richardson model where S vanishes at infinite coupling strength [27], here we observe that $S \approx [1 + 3.3(g_c/W)^2]/[1 + 37.4(g_c/W)^2]$, reaching a positive constant when $g_c \gg W$.

Integrability-breaking perturbations. So far we have focused on the TC Hamiltonian (1), known to be integrable, and we found Poisson level statistics, multifractality, and absence of thermalization signaled by the non-vanishing EA parameter. We now ask: Do these features survive integrability-breaking perturbations? To check

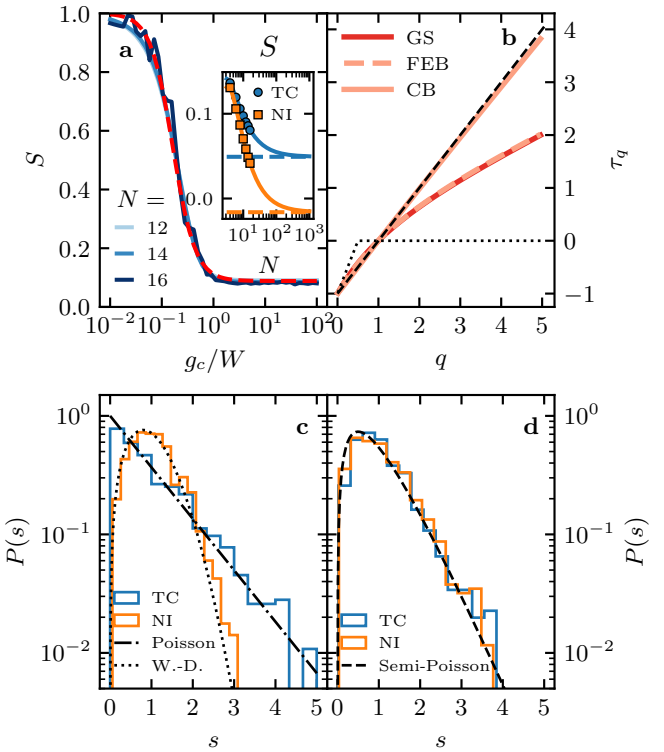


FIG. 3. **a** Long-time survival probability S [Eq. (7)], against the collective coupling strength g_c . The dashed line is the best fit with $[1 + A(g_c/W)^2]/[1 + B(g_c/W)^2]$, where $A = 3.3$ and $B = 37.4$. Inset: extrapolation of S to the thermodynamic limit (dashed lines) by the finite- N scaling $S(N) = S + c_1/N + c_2/N^2$ (continuous lines, adapted from Ref. [27]), both for the integrable case [TC: Eq. (1), $g_c/W = 10$] and for the non-integrable case [NI: Eq. (8), $g_c/W = 10$ and $J/W = 0.1$]. **b** Fitted exponent τ_q as a function of q in the non-integrable Hamiltonian (8) for different energy bands (see legend), with $g_c/W = 10$ and $J/W = 0.1$. GS's and FEB's data are overlapping. Black dashed line: fully extended case ($\tau_q = q - 1$), dotted line: single-excitation case ($\tau_q = \min(2q - 1, 0)$). **c,d** Probability density function $P(s)$ of the normalized level spacing s at half filling ($N = 14$, $M = 7$) and strong coupling ($g_c/W = 10$) for the CB (c) and FEB (d), for the integrable (TC) and non-integrable (NI) case ($J/W = 0.1$). “W.-D.”: Wigner-Dyson distribution.

this, we add a small nearest-neighbour hopping term

$$H_{\text{NI}} = H_{\text{TC}} + J \sum_{n=1}^{N-1} (\sigma_n^+ \sigma_{n+1}^- + \sigma_n^- \sigma_{n+1}^+), \quad (8)$$

with $J \ll W, g_c$. We find that even a very small hopping ($J/W = 0.1$ with $g_c/W = 10$) is enough to change all the properties of the CB: the level statistics changes from Poisson to Wigner-Dyson (see Fig. 3c, with level spacing ratio $\langle r \rangle = 0.549 \pm 0.007$), the survival probability tends to zero once extrapolated to the thermodynamic limit (see inset of Fig. 3a, non-integrable NI compared to the integrable TC model), and the eigen-

states become ergodic (see Fig. 3b). The multifractality of the GS and FEB and the semi-Poisson statistics of the FEB remain unaffected by nearest-neighbor hopping, see Fig. 3b,d, respectively. The same robustness to nearest-neighbour hopping has been observed in the non-interacting case [25], and it is consistent with the fact that the FEB reflects ‘single-particle physics’, since its eigenstates are constituted by one dark state and $M - 1$ robust polaritons.

Proposal for an experimental realization with cold atoms. We propose to implement the model using hyperfine states of alkali atoms trapped in a high finesse cavity. Disorder would be imprinted using a laser with randomly distributed intensity, inducing a vector light-shift of the ground hyperfine manifold. This can be achieved with the lowest spontaneous emission for the heaviest alkalis such as Rb and Cs. Considering for concreteness ^{87}Rb as in [43], the two-level system can be encoded using the $|F = 1, m_F = 1\rangle$ and $|F = 2, m_F = 2\rangle$ levels. Circularly polarized light incident from the side at the wavelength of 795 nm, either forming an incommensurate lattice like in [44] or a speckle pattern, will induce a random effective magnetic field with tunable strength. Raman coupling involving cavity photons in one arm yields then a realization of the random Tavis-Cummings model, with an effective tunable g_c and a long lifetime, limited only by the spontaneous emission [45].

The atoms can be prepared into a coherent spin state at the equator of the collective Bloch sphere, realizing a coherent superposition of excitations close to half-filling. The time-evolution of the spin polarization can then be monitored in time and even in space if the spins are individually addressable [46, 47]. As shown in [44], the participation ratio in the linear regime can be estimated from response functions, and it would be interesting to explore possible extensions to the interacting case.

Last, the open character of cavity QED platforms will lead to dissipation. The finite photon lifetime will set an upper bound to the experimentally accessible timescales during which the system possesses a fixed number of excitations. Very narrow cavities with Rb atoms in the strong coupling regime have been demonstrated with photon lifetimes up to $35\ \mu\text{s}$ [48], which could be leveraged to ensure the largest intrinsic lifetime. Beyond this timescale, continuous pumping would then be needed to stabilize the system around an average number of excitations. The use of long-lived atomic states will ensure that dissipation is predominantly due to photons leaking from the cavity, which can then be detected. In particular, the super-radiant emission expected for fully-delocalized excitations may bear the signature of the multifractal character of the excitations when disorder is increased.

Discussion and outlook. The results above imply that the eigenfunctions are partially delocalized even if the level statistics suggests otherwise, thus favouring exciton transport. Moreover, cavity-mediated interactions be-

tween the excitons favor delocalization of the wave functions both in the integrable and non-integrable models (see Figs. 2 and 3b). In the former, this is associated with a change in the exponent τ_q which is positive for $q > 1$, as opposed to the frozen phase observed in the non-interacting case (see Fig. 2b). As a consequence, the many-body interactions seem to make the eigenfunctions more delocalized, *i.e.* more similar to those of a good conductor. The effects of interactions are also striking in the non-integrable case as they appear to turn the system into a perfect conductor at finite energy. This is in stark contrast to the non-interacting single-excitation model, where multifractality is robust to nearest-neighbor hopping perturbations at all energies [25].

Those described above are examples of qualitative modifications in the many-particle eigenfunctions due to collective light-matter coupling of spins to the photon field, resulting in new transport properties and phases of matter – a result relevant to the growing field of light-modified quantum matter [49, 50]. They might find direct applications in improving exciton conductivity in, *e.g.*, disordered molecular systems, where it has recently been observed that a strong collective light-matter coupling to a cavity field strongly boosts the diffusion coefficient, even inducing ballistic transport [51, 52].

We acknowledge useful discussions with Jakob Reichel, Romain Long, Dmitry Abanin, Alexandre Faribault, Ivan Khaymovich and Felipe Herrera. This work has benefited from state grants managed by the French National Research Agency under the Investments of the Future Program with the reference ANR-21-ESRE-0032, and by the ANR project CLIMAQS. We acknowledge support from ECOS-CONICYT through project nr. C20E01 and the CNRS through the IEA 2020 campaign. Computing time was provided by the High Performance Computing Center of the University of Strasbourg. JPB acknowledges funding from the Swiss National Science Foundation (grant No 184654) and the Swiss State Secretariat for Education, Research and Innovation (grant MB22.00063).

- [1] T. C. Halsey, M. H. Jensen, L. P. Kadanoff, I. Procaccia, and B. I. Shraiman, *Phys. Rev. A* **33**, 1141 (1986).
- [2] J.-S. Gagnon, S. Lovejoy, and D. Schertzer, *Nonlinear Proc. Geoph.* **13**, 541 (2006).
- [3] C. Meneveau and K. R. Sreenivasan, *J. Fluid Mech.* **224**, 429–484 (1991).
- [4] P. C. Ivanov, L. A. N. Amaral, A. L. Goldberger, S. Havlin, M. G. Rosenblum, Z. R. Struzik, and H. E. Stanley, *Nature* **399**, 461 (1999).
- [5] B. B. Mandelbrot, *Sci. Am.* **280**, 70 (1999).
- [6] P. W. Anderson, *Phys. Rev.* **109**, 1492 (1958).
- [7] F. Evers and A. D. Mirlin, *Rev. Mod. Phys.* **80**, 1355 (2008).
- [8] J. Dubail, T. Botzung, J. Schachenmayer, G. Pupillo,

and D. Hagenmüller, *Phys. Rev. A* **105**, 023714 (2022).

[9] B. I. Shklovskii, B. Shapiro, B. R. Sears, P. Lambrianides, and H. B. Shore, *Phys. Rev. B* **47**, 11487 (1993).

[10] E. B. Bogomolny, U. Gerland, and C. Schmit, *Phys. Rev. E* **59**, R1315 (1999).

[11] E. J. Torres-Herrera and L. F. Santos, *Phys. Rev. B* **92**, 014208 (2015).

[12] N. Macé, F. Alet, and N. Laflorencie, *Phys. Rev. Lett.* **123**, 180601 (2019).

[13] K. S. Tikhonov and A. D. Mirlin, *Phys. Rev. B* **97**, 214205 (2018).

[14] D. J. Luitz, I. M. Khaymovich, and Y. B. Lev, *SciPost Phys. Core* **2**, 006 (2020).

[15] G. De Tomasi, I. M. Khaymovich, F. Pollmann, and S. Warzel, *Phys. Rev. B* **104**, 024202 (2021).

[16] C. Monthus, *J. Phys. A: Math. Theor.* **50**, 295101 (2017).

[17] I. M. Khaymovich, V. E. Kravtsov, B. L. Altshuler, and L. B. Ioffe, *Phys. Rev. Research* **2**, 043346 (2020).

[18] G. Biroli and M. Tarzia, *Phys. Rev. B* **103**, 104205 (2021).

[19] A. Bäcker, M. Haque, and I. M. Khaymovich, *Phys. Rev. E* **100**, 032117 (2019).

[20] M. Tavis and F. W. Cummings, *Phys. Rev.* **170**, 379 (1968).

[21] V. V. Temnov and U. Woggon, *Phys. Rev. Lett.* **95**, 243602 (2005).

[22] M. H. Szymańska, J. Keeling, and P. B. Littlewood, *Phys. Rev. Lett.* **96**, 230602 (2006).

[23] I. Diniz, S. Portolan, R. Ferreira, J. M. Gérard, P. Bertet, and A. Auffeves, *Phys. Rev. A* **84**, 063810 (2011).

[24] M. Tokman, A. Behne, B. Torres, M. Erukhimova, Y. Wang, and A. Belyanin, *Phys. Rev. A* **107**, 013721 (2023).

[25] T. Botzung, D. Hagenmüller, S. Schütz, J. Dubail, G. Pupillo, and J. Schachenmayer, *Phys. Rev. B* **102**, 144202 (2020).

[26] W. Tang and I. M. Khaymovich, *Quantum* **6**, 733 (2022).

[27] F. Buccheri, A. De Luca, and A. Scardicchio, *Phys. Rev. B* **84**, 094203 (2011).

[28] A. Pal and D. A. Huse, *Phys. Rev. B* **82**, 174411 (2010).

[29] J. Z. Imbrie, V. Ros, and A. Scardicchio, *Ann. Phys.* **529**, 1600278 (2017).

[30] I. V. Gornyi, A. D. Mirlin, and D. G. Polyakov, *Phys. Rev. Lett.* **95**, 206603 (2005).

[31] D. M. Basko, I. L. Aleiner, and B. L. Altshuler, *Ann. Phys.* **321**, 1126 (2006).

[32] D. J. Luitz, N. Laflorencie, and F. Alet, *Phys. Rev. B* **91**, 081103 (2015).

[33] The level spacing ratio of the semi-Poisson distribution ($\langle r \rangle = 0.6137 \pm 0.0003$) has been computed by generating 10^6 uniformly distributed random numbers and collecting the middle points of each pair of neighbouring numbers.

[34] V. Oganesyan and D. A. Huse, *Phys. Rev. B* **75**, 155111 (2007).

[35] F. Alet and N. Laflorencie, *C. R. Phys. Quantum simulation / Simulation quantique*, **19**, 498 (2018).

[36] X. Deng, G. Masella, G. Pupillo, and L. Santos, *Phys. Rev. Lett.* **125**, 010401 (2020).

[37] M. Gaudin, *Journal de Physique* **37**, 1087 (1976).

[38] H. Tschirhart and A. Faribault, *J. Phys. A: Math. Theor.* **47**, 405204 (2014).

[39] H. Tschirhart, *From two Algebraic Bethe Ansätze to the dynamics of Dicke-Jaynes-Cummings-Gaudin quantum integrable models through eigenvalue-based determinants*, Ph.D. thesis, Université de Lorraine (2017).

[40] P. W. Claeys, *Richardson-Gaudin models and broken integrability*, Ph.D. thesis, Ghent University (2018).

[41] H. Tschirhart, T. Platini, and A. Faribault, *J. Stat. Mech: Theory Exp.* **2018**, 083102 (2018).

[42] L.-H. Tang, D. M. Long, A. Polkovnikov, A. Chandran, and P. W. Claeys, Integrability and quench dynamics in the spin-1 central spin XX model (2022), [arXiv:2212.04477 \[cond-mat\]](https://arxiv.org/abs/2212.04477).

[43] M. Baghdad, P.-A. Bourdel, S. Schwartz, F. Ferri, J. Reichenel, and R. Long, Spectral Engineering of Cavity-Protected Polaritons in an Atomic Ensemble with Controlled Disorder (2022), [arXiv:2208.12088 \[quant-ph\]](https://arxiv.org/abs/2208.12088).

[44] N. Sauerwein, F. Orsi, P. Uhrich, S. Bandyopadhyay, F. Mattiotti, T. Cantat-Moltrecht, G. Pupillo, P. Hauke, and J.-P. Brantut, Engineering random spin models with atoms in a high-finesse cavity (2022), [arXiv:2208.09421 \[cond-mat, physics:physics, physics:quant-ph\]](https://arxiv.org/abs/2208.09421).

[45] J. G. Bohnet, Z. Chen, J. M. Weiner, D. Meiser, M. J. Holland, and J. K. Thompson, *Nature* **484**, 78 (2012).

[46] E. Deist, J. A. Gerber, Y.-H. Lu, J. Zeiher, and D. M. Stamper-Kurn, *Phys. Rev. Lett.* **128**, 083201 (2022).

[47] Y. Liu, Z. Wang, P. Yang, Q. Wang, Q. Fan, G. Li, P. Zhang, and T. Zhang, Realization of strong coupling between deterministic single-atom arrays and a high-finesse miniature optical cavity (2022), [arXiv:2207.04371 \[quant-ph\]](https://arxiv.org/abs/2207.04371).

[48] M. Wolke, J. Klinner, H. Keßler, and A. Hemmerich, *Science* **337**, 75 (2012).

[49] F. J. Garcia-Vidal, C. Ciuti, and T. W. Ebbesen, *Science* **373**, eabd0336 (2021).

[50] M. Ruggenthaler, N. Tancogne-Dejean, J. Flick, H. Appel, and A. Rubio, *Nat Rev Chem* **2**, 0118 (2018).

[51] M. Balasubrahmanyam, A. Simkhovich, A. Golombok, G. Sandik, G. Ankonina, and T. Schwartz, *Nat. Mater.* **10**, 1038/s41563-022-01463-3 (2023).

[52] K. Nagarajan, J. George, A. Thomas, E. Devaux, T. Chervy, S. Azzini, K. Joseph, A. Jouaiti, M. W. Hosseini, A. Kumar, C. Genet, N. Bartolo, C. Ciuti, and T. W. Ebbesen, *ACS Nano* **14**, 10219 (2020).